Journal of Materials Research and Technology 28 (2024) 4250–4261

Contents lists available at ScienceDirect

Journal of Materials Research and Technology

journal homepage: www.elsevier.com/locate/jmrt

Twinning-assisted static recrystallization and texture evolution in a Mg-Gd-Y-Zr alloy

Wenting Jiang [a], Xinyu Ren [a], Lei Yu [a], Jingli Sun [b], Song Ni [a,*], Yi Huang [c,d], Min Song [a]

[a] State Key Laboratory of Powder Metallurgy, Central South University, Changsha, 410083, China
[b] Shanghai Spaceflight Precision Machinery Institute, Shanghai, 201600, China
[c] Department of Design and Engineering, Faculty of Science and Technology, Bournemouth University, Poole, Dorset, BH12 5BB, UK
[d] Materials Research Group, Department of Mechanical Engineering, University of Southampton, Southampton, SO17 1BJ, UK

ARTICLE INFO

Keywords:
Mg-Gd-Y-Zr alloy
Recrystallization
Twinning
Texture

ABSTRACT

The formability and mechanical properties of magnesium (Mg) alloys are strongly related to the crystallographic basal texture. Twins play critical roles in adjusting crystallographic orientation of grains during both deformation and annealing treatment via deformation twinning and twinning-assisted recrystallization. In this study, cold rolling and subsequent annealing were conducted on a Mg-5.9Gd-3.3Y-0.5Zr alloy to investigate the recrystallization behavior and texture evolution. Electron backscatter diffraction and transmission electron microscopy techniques were applied to characterize the nucleation of recrystallized grains, especially the twinning-assisted recrystallization, at multi-scales. The results indicated that a large number of $\{10\bar{1}2\}$, $\{10\bar{1}1\}$ twins and $\{10\bar{1}1\}$-$\{10\bar{1}2\}$ double twins were introduced after cold rolling. The $\{10\bar{1}1\}$-$\{10\bar{1}2\}$ double twins, double twin - grain boundary intersections and dense twin-twin intersections acted as the preferential nucleation sites for recrystallization during annealing treatment, while the coarse and parallel $\{10\bar{1}2\}$ twins were unfavorable for the nucleation of recrystallized grains. Although $\{10\bar{1}2\}$ tension twins are the most common twins in Mg alloys, the interface of this type of twin has strong mobility and is easy to expand. Therefore, it is generally difficult for a single $\{10\bar{1}2\}$ twin to recrystallize. However, the $\{10\bar{1}1\}$ compression twins and $\{10\bar{1}1\}$-$\{10\bar{1}2\}$ double twins are generally difficult to expand and can store high deformation energy, so they are conducive to becoming nucleation sites for recrystallization. During the recrystallization process, the texture type (basal texture) of the cold rolled sample remained unchanged, but the overall texture intensity was significantly reduced due to the dispersion of grain orientations brought by new grains generated by twinning recrystallization.

1. Introduction

As the lightest structural metals, Magnesium (Mg) and its alloys, especially Mg alloys containing rare earth (RE) elements such as Mg–Gd, Mg–Y and Mg-Gd-Y series alloys have drawn wide attention in the fields of aerospace and automotive industries due to their high strength and good heat resistance [1–4]. Among various strengthening mechanisms, grain refinement strengthening is considered to be a promising way to improve the mechanical properties [5–8]. By combining plastic deformation with subsequent annealing treatment can acquire fine grains and weaken the texture via recrystallization in Mg alloys [9–11].

In deformed Mg alloys, deformation twins, grain boundaries, shear bands and precipitates are the proposed nucleation sites for recrystallization [12–14]. Among which, deformation twins play critical roles in adjusting crystallographic orientation of grains during both deformation and annealing treatments due to the limited number of independent slip systems in hexagonal close-packed (HCP) metals [15–20]. The $\{10\bar{1}2\}\langle 10\bar{1}1 >$ tension twins, $\{10\bar{1}1\}\langle 10\bar{1}2 >$ compression twins, and $\{10\bar{1}1\} - \{10\bar{1}2\}$ double twins are the commonly observed twins in Mg alloys [21–24]. The twin types, twin variants, twin-twin and twin-grain boundary intersections affect the recrystallization behaviors. Recrystallization within $\{10\bar{1}1\}$ compression twins and $\{10\bar{1}1\} - \{10\bar{1}2\}$ double twins has been frequently observed and reported due to the basal dislocation slip which occurs easily within these twins and the high stored energy [25–29]. The $\{10\bar{1}2\}\langle 10\bar{1}1 >$ tension twins can be activated easily at the early stage of deformation due to the low critical resolved shear stress [22], but it is controversial whether the $\{10\bar{1}2\}$

* Corresponding author.
E-mail address: song.ni@csu.edu.cn (S. Ni).

https://doi.org/10.1016/j.jmrt.2024.01.007
Received 29 October 2023; Received in revised form 23 December 2023; Accepted 2 January 2024
Available online 3 January 2024

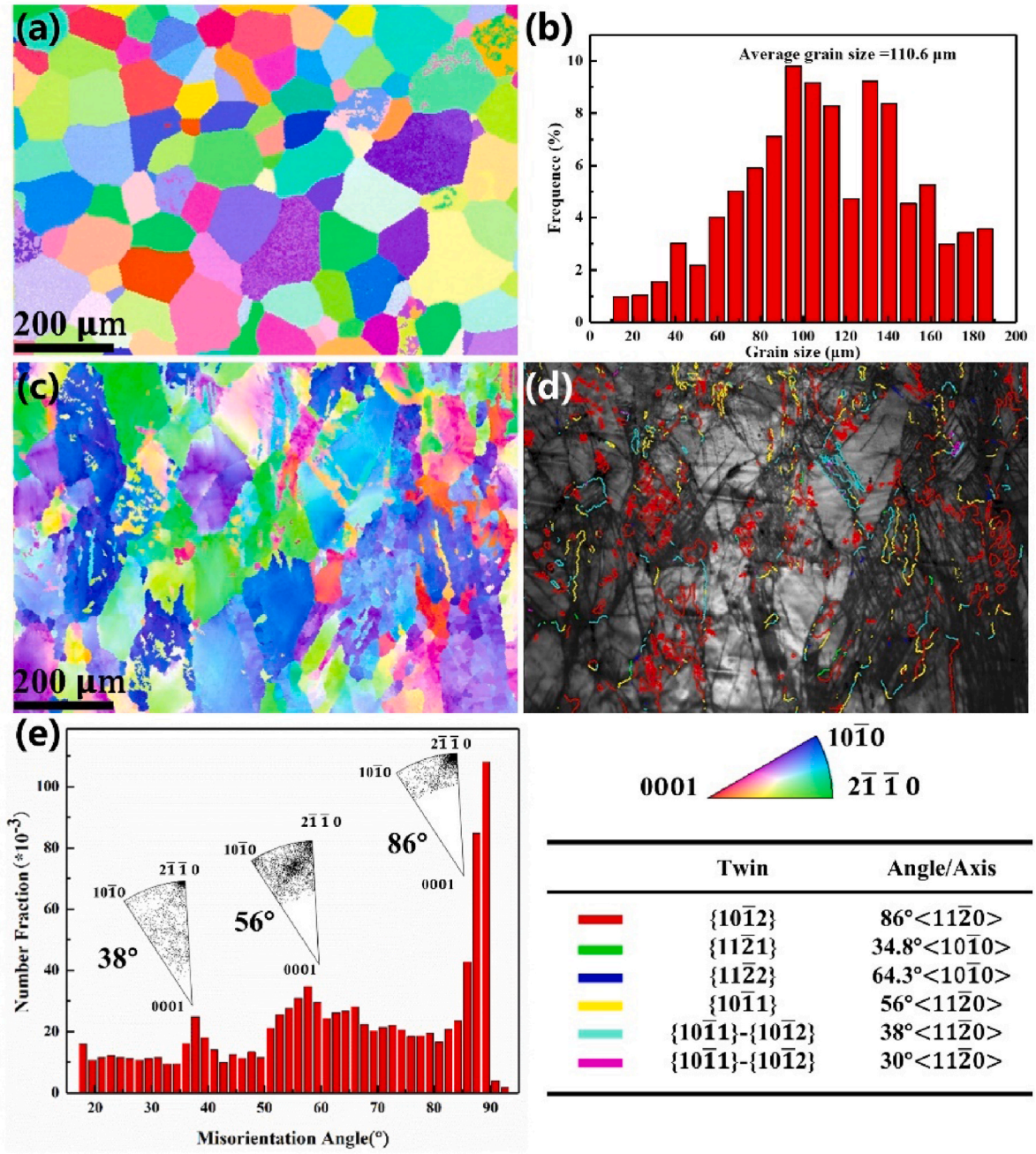

	Twin	Angle/Axis
	{10$\bar{1}$2}	86°<11$\bar{2}$0>
	{11$\bar{2}$1}	34.8°<10$\bar{1}$0>
	{11$\bar{2}$2}	64.3°<10$\bar{1}$0>
	{10$\bar{1}$1}	56°<11$\bar{2}$0>
	{10$\bar{1}$1}-{10$\bar{1}$2}	38°<11$\bar{2}$0>
	{10$\bar{1}$1}-{10$\bar{1}$2}	30°<11$\bar{2}$0>

Fig. 1. The EBSD results of the homogenized (a, b) and cold rolled (c–e) samples. (a) IPF map, (b) grain size distribution bar graph, (c) IPF map, (d) IQ map superimposed with the boundary map, (e) the distribution of misorientation angles of grain boundaries.

twins can be the preferred nucleation sites for recrystallization. Some researchers [23,25,30] reported that {10$\bar{1}$2} twins are unfavorable for the nucleation and growth of recrystallized grains due to the low Schmidt factor for basal slip within the twins and the low stored energy. Guan et al. [30] reported that no recrystallization occurred in both {10$\bar{1}$2} twins and twin-twin intersections, while double twins acted as the preferred nucleation sites for recrystallization and contributed greatly to the recrystallization process. However, Lu et al. [31] reported that by activating a large number of randomly orientated and interacted {10$\bar{1}$2} twins via multi-directional forging, these {10$\bar{1}$2} twins can also serve as nucleation sites for static recrystallization after accumulating sufficient strain energy.

Recrystallized grains originating from twins can scatter and randomize the grain orientation, which is considered capable of weakening the deformed texture. However, the understanding on the contribution of twin recrystallization to texture modification is still controversial. Some researchers [25,32,33] reported that the recrystallized grains nucleating inside twins did not grow beyond the twin size, resulting a limited texture weakening effect on the original deformed microstructure. Lu et al. [9] also reported that most recrystallized grains maintained the original grain orientations and no obvious difference was shown on the texture evolution during annealing treatment. However, other researchers [30] found that recrystallized grains, originating from double twins made the main contribution to texture modification and concluded that recrystallization from double twins and double twin - grain boundary intersections exhibited a weak, non-basal texture. Liu et al. [34] also reported a significantly weakened basal texture due to strong orientation scattering by the recrystallized grains in compression and double twins in a Mg–Zn alloy. It is therefore crucial to figure out the

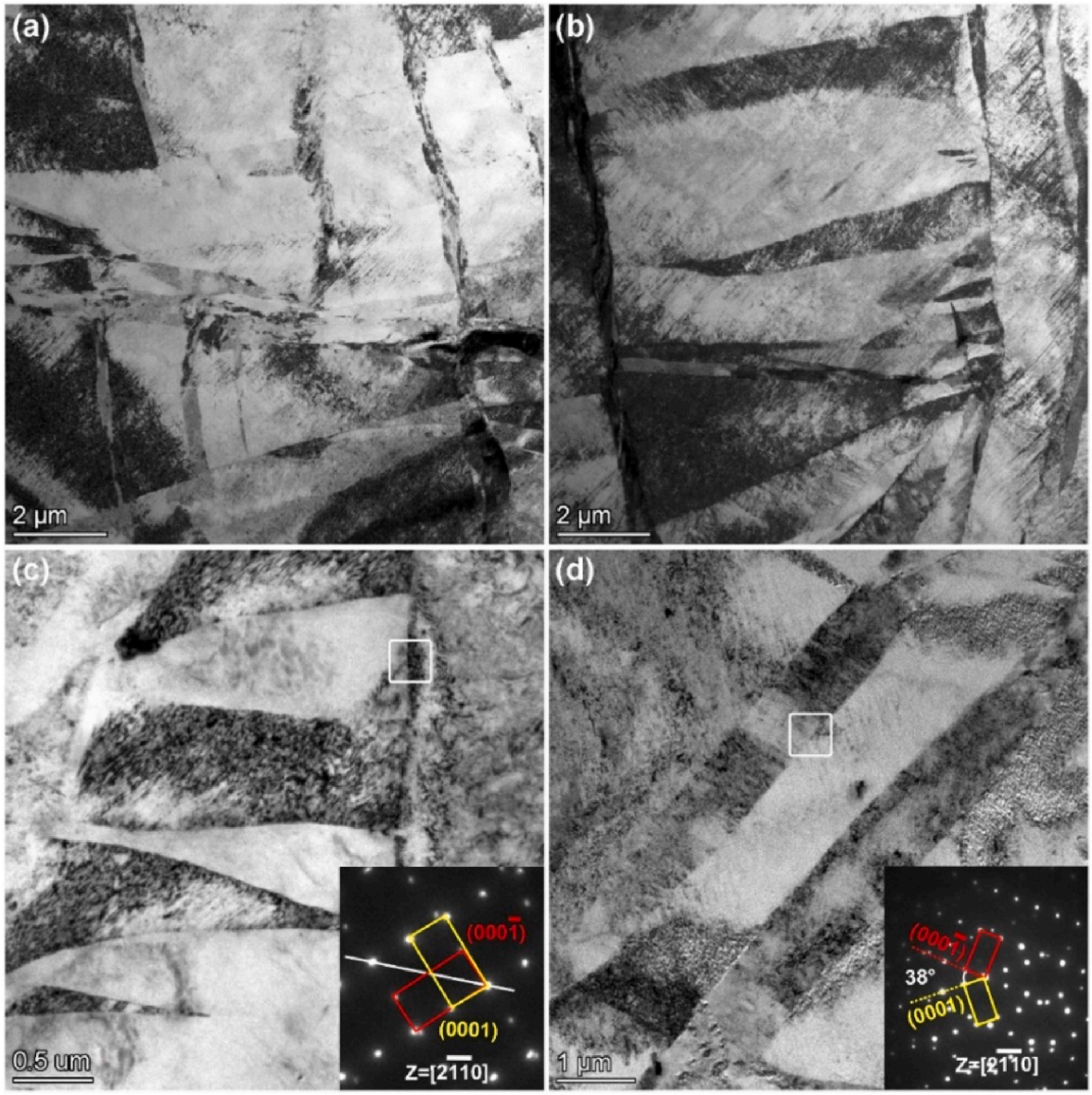

Fig. 2. (a, b) Typical bright-field TEM images of the cold rolled sample. (c, d) The bright-filed TEM images and the corresponding SAED patterns of the squared areas.

different recrystallization behaviors as a function of twin types and their contribution to texture evolution.

In this work we examined the recrystallization process during isothermal annealing of a cold-rolled Mg-5.9Gd-3.3Y-0.5Zr alloy. Optical microscope (OM), electron back-scatter diffraction (EBSD) and transmission electron microscopy (TEM) characterizations were conducted to reveal the recrystallization behaviors as a function of twin types at multi-scales. Various types of twins were introduced after cold rolling. The $\{10\bar{1}1\}$-$\{10\bar{1}2\}$ double twins, double twin - grain boundary intersections and dense twin-twin intersections acted as the preferential nucleation sites for recrystallization during annealing treatment, while the coarse and parallel $\{10\bar{1}2\}$ twins were unfavorable for the nucleation of recrystallized grains. The texture intensity was significantly reduced due to the dispersion of grain orientations brought by new grains generated by twinning recrystallization.

2. Experimental procedures

The material used in the present study was a Mg-Gd-Y-Zr alloy prepared by casting method. The chemical composition was determined to be Mg-5.9Gd-3.3Y-0.5Zr (wt.%) by using inductively coupled plasma mass spectroscopy (ICP-MS). Samples with dimensions of 10 mm × 60 mm × 70 mm were machined from the cast ingot by wire electrode cutting, and then homogenized at 520 °C for 12 h and cooled in water. These homogenized samples were cold rolled with a thickness reduction of 0.5 mm for each pass. In favor of investigating the recrystallization behaviors as a function of twin types, a total thickness reduction of 30 % was employed to activate a certain number of twins in different types and orientations. The rolled samples were annealed in air at 400 °C for 1 min, 3 min, 4 min, 5 min, 10 min and 20 min, respectively, followed by rapid quenching in water.

An HVS-1000M2 Vickers micro-hardness tester was used to measure the hardness of the cold-rolled and annealed samples with a load of 100 g holding for 15 s. The microhardness value for each sample was averaged from every 5 points. The microstructure and texture evolution were characterized using optical microscopy, scanning electron microscopy (SEM, FEI Helios NanoLab G3 UC) equipped with an electron backscatter diffraction detector (EBSD) and transmission electron microscopy (TEM, FEI Titan 60–300 operating at 200 KV). The surfaces along the transverse direction of all samples were characterized. The TSL OIM

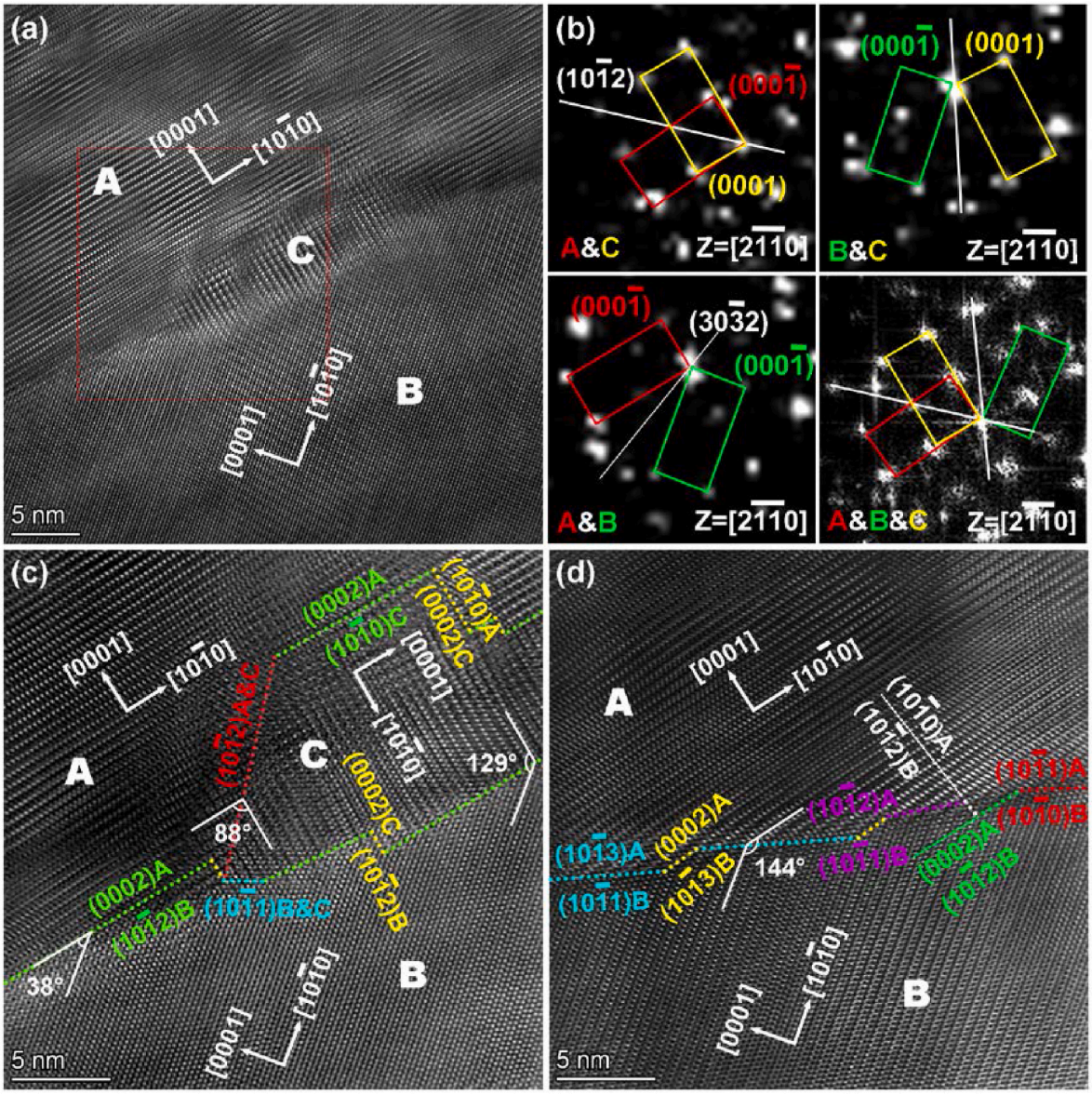

Fig. 3. (a, b) An HRTEM image of a 38° {10$\bar{1}$1}-{10$\bar{1}$2} double twin and FFT patterns containing the interfaces of areas A and C, B and C, A and B, and the whole area, (c, d) magnified HRTEM images along the twin boundary in (a).

software was used to acquire pseudo-colored orientation imaging microscopy. Specimens for OM observation were prepared by conventional grinding with SiC papers from 400 to 2000 grit and diamond polishing from W2.5 to W0.5, followed by corroding in 4 % sodium citrate solution for 40–60 s. Specimens for EBSD observation were prepared by grinding and diamond polishing and then subjected to electrochemical polishing in a mixed solution of perchloric acid (2 vol%) and ethanol (98 vol%) at a voltage of 25 V and a temperature of −35 °C for 2 min. For TEM analysis, foils after mechanical grinding with a thickness of 50 μm were twin-jet electropolished in a mixture of perchloric acid (3 vol%) and ethanol (97 vol%) at a voltage of 35 V and a temperature of −35 °C.

3. Results

3.1. Microstructure of the cold rolled Mg-Gd-Y-Zr alloy

Fig. 1 shows the microstructures of the homogenized (a, b) and cold rolled (c-e) alloy samples. Fig. 1a and b are the inverse pole figure (IPF) map and grain size distribution histogram of the homogenized sample. The average grain size was measured to be ~110.6 μm after homogenization. Fig. 1c and d presents the IPF map and image quality (IQ) map superimposed with the boundary map of the cold rolled sample. From Fig. 1d, the {10$\bar{1}$2}, {11$\bar{2}$1}, {11$\bar{2}$2}, {10$\bar{1}$1} and {10$\bar{1}$1}-{10$\bar{1}$2} twin boundaries marked with different colors were detected. Among them, {10$\bar{1}$2}, {10$\bar{1}$1} twins and {10$\bar{1}$1}-{10$\bar{1}$2} double twins indicated by red, yellow and cyan blue lines, respectively, were the dominant twinning types. From Fig. 1e–a large number of high angle grain boundaries existed in the cold rolled sample. The distribution peaks of misorientation angles at around 38°, 56° and 86° corresponded to the {10$\bar{1}$1-{10$\bar{1}$2} double twins, {10$\bar{1}$1} compression twins and {10$\bar{1}$2} tension twins, respectively.

Fig. 2 shows the typical bright-field TEM images of the cold rolled sample. A high density of twins, double twins and twin-twin intersections were observed in Fig. 2a and b. Fig. 2c and d are bright-filed TEM images and the corresponding selected area electron diffraction (SAED) patterns of the squared areas, which indicate the presence of a 86° {10$\bar{1}$2} twin and a 38° {10$\bar{1}$1}-{10$\bar{1}$2} double twin. The double twin was further characterized via high-resolution TEM (HRTEM). Fig. 3a

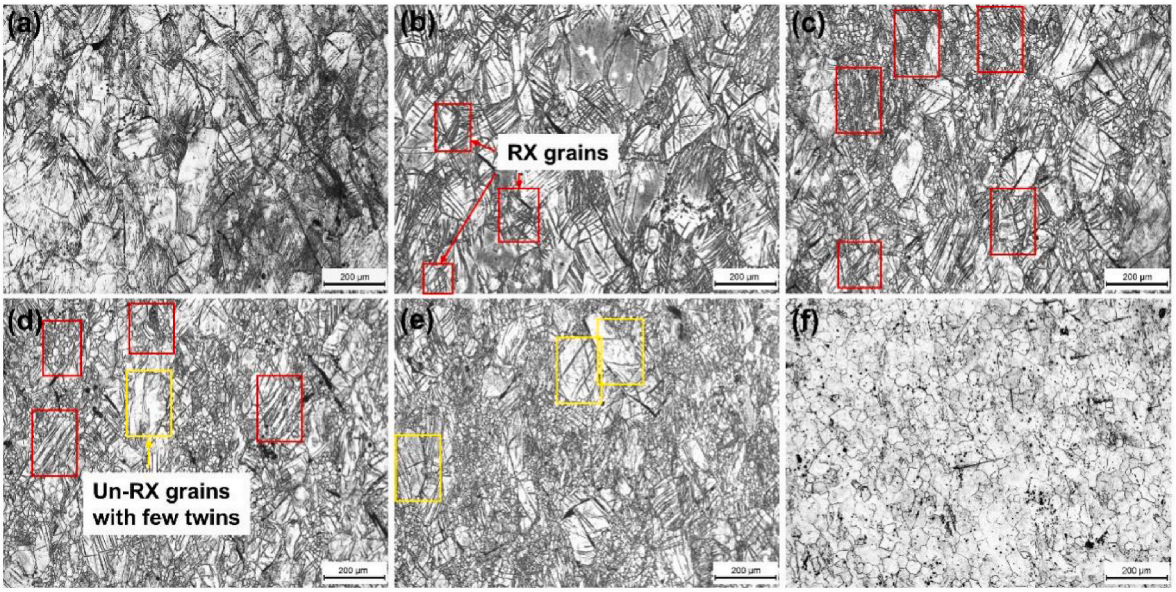

Fig. 4. The OM images of cold-rolled sample after annealing at 400 °C for (a) 1 min, (b) 3 min, (c) 4 min, (d) 5 min, (e) 10 min, (f) 20 min.

shows an HRTEM image of a selected area along a typical 38° $\{10\bar{1}1\}$-$\{10\bar{1}2\}$ double twin boundary. It's interesting that areas A, B and C with different HCP lattice orientations were observed. Fig. 3b shows the fast Fourier transformation (FFT) patterns containing the interfaces of A and C, B and C, A and B, and the whole area, with the diffraction spots of regions A, B and C marked by red, green and yellow boxes, respectively, which show symmetric relations under $[2\bar{1}\bar{1}0]$ zone axis. The symmetric relations of the FFT patterns containing different areas indicate different twinning relations, such as, a 86° $\{10\bar{1}2\}$ twin relation exists between A and C, a 56° $\{10\bar{1}1\}$ twin relation exists between B and C, and a 38° $\{10\bar{1}1\}$-$\{10\bar{1}2\}$ double twin relation exists between A and B. Such twinning relations were further confirmed by the magnified HRTEM images along the twin boundary, as shown in Fig. 3c and d. The lattices in A and C present a symmetric relation with $\{10\bar{1}2\}$ plane as the symmetric plane (as indicated by the red dotted line), and the lattices in B and C show a symmetric relation about $\{10\bar{1}1\}$ plane (as shown by the cyan dotted line). Firstly, a 56° $\{10\bar{1}1\}$ twinning occurred between area B and area C, then a 86° $\{10\bar{1}2\}$ twinning occurred between area A and area C, and area C was subsequently consumed, which eventually resulted the formation of a 38° $\{10\bar{1}1\}$-$\{10\bar{1}2\}$ double twin relation between A and B. Zigzag steps can be observed along the double twin boundaries to accommodate the orientation, as shown in Fig. 3c and d.

3.2. Microstructural evolution during annealing treatment

The cold rolled samples were annealed at 400 °C to different time to investigate the effects of deformation twins on the static recrystallization behaviors and texture evolution. Fig. 4 displays a series of OM images of the cold rolled samples after annealing for different time. After 1 min and 3 min annealing, as shown in Fig. 4a and b, a high density of deformation twins were retained and only a few recrystallized grains were observed in local areas. After 4 min and 5 min annealing, obvious recrystallization occurred, consuming the deformed twins gradually. Some recrystallized regions and several regions without obvious recrystallized grains were marked by red and yellow rectangles, respectively. Notice that the unrecrystallized grains show relatively few twins. When the annealing time reached 20 min, the original deformed grains were completely transformed into recrystallized grains with the average grain size of ~40–50 nm, as shown in Fig. 4f.

Fig. 5 shows the EBSD IPF maps and grain orientation spread (GOS) maps of the cold-rolled samples after annealing at 400 °C for different time. In the GOS maps, fully recrystallized grains (GOS <2°), partially recrystallized grains (2° < GOS <5°) and un-recrystallized grains (5° < GOS) were defined by the different GOS values, and the area fractions of them were indicated by the blue, yellow and red colors, respectively. Very few fully recrystallized grains were detected in 1 min annealed sample, as shown in Fig. 5b. As the annealing time increased to 5 min (Fig. 5h), the fraction of fully recrystallized grains increased from 0.2 % to 40.8 %.

Fig. 6 shows the further EBSD characterization results of the cold rolled alloy after annealing for 5 min. It can be seen from the IPF image that obvious recrystallization occurred in the sample. The $\{10\bar{1}2\}$ twins and $\{10\bar{1}1\}$-$\{10\bar{1}2\}$ double twins were the main twins as seen from the IQ map in Fig. 6b. Areas c, d and e in Fig. 6a were further enlarged in Fig. 6c–e, respectively. Many 38° $\{10\bar{1}1\}$-$\{10\bar{1}2\}$ double twins and a few 86° $\{10\bar{1}2\}$ twins were observed in Fig. 6c and d, while many 86° $\{10\bar{1}2\}$ twins and very few 38° $\{10\bar{1}1\}$-$\{10\bar{1}2\}$ double twins were observed in Fig. 6e. Recrystallized grains were observed at areas c and d but rarely observed at area e. It can be seen that the recrystallized grains preferentially formed at the 38° $\{10\bar{1}1\}$-$\{10\bar{1}2\}$ double twin boundaries during the initial annealing treatment.

In order to further understand the relation between the deformed microstructure, especially the deformation twins, and the recrystallization behaviors, TEM analysis was conducted on the annealed specimens. Fig. 7 shows TEM images of the annealed specimen, from which recrystallized grains mainly distributed along twin boundaries were observed. The diffraction pattern in Fig. 7a shows a tendency to ring, indicating a large number of recrystallized grains in this region. Symmetric relations can be found between some spots, as indicated by the rectangles. In Fig. 7b–a $\{10\bar{1}1\}$-$\{10\bar{1}2\}$ double twin can be indexed from the diffraction pattern taken from the pointed area and several recrystallized grains were formed within the double twin. Besides, a high density of dislocations and dislocation substructures were also observed in Fig. 7a and b, which were formed due to the deformation induced dislocation generation, accumulation and annealing induced recovery effect.

The twinning recrystallization shown in Fig. 7b was further analyzed in Fig. 8. Grains A-G were labeled in Fig. 8a. HRTEM images containing interfaces of these grains as marked by squares and their corresponding FFT patterns were shown in Fig. 8c–g. As shown in Fig. 8c, the matrix

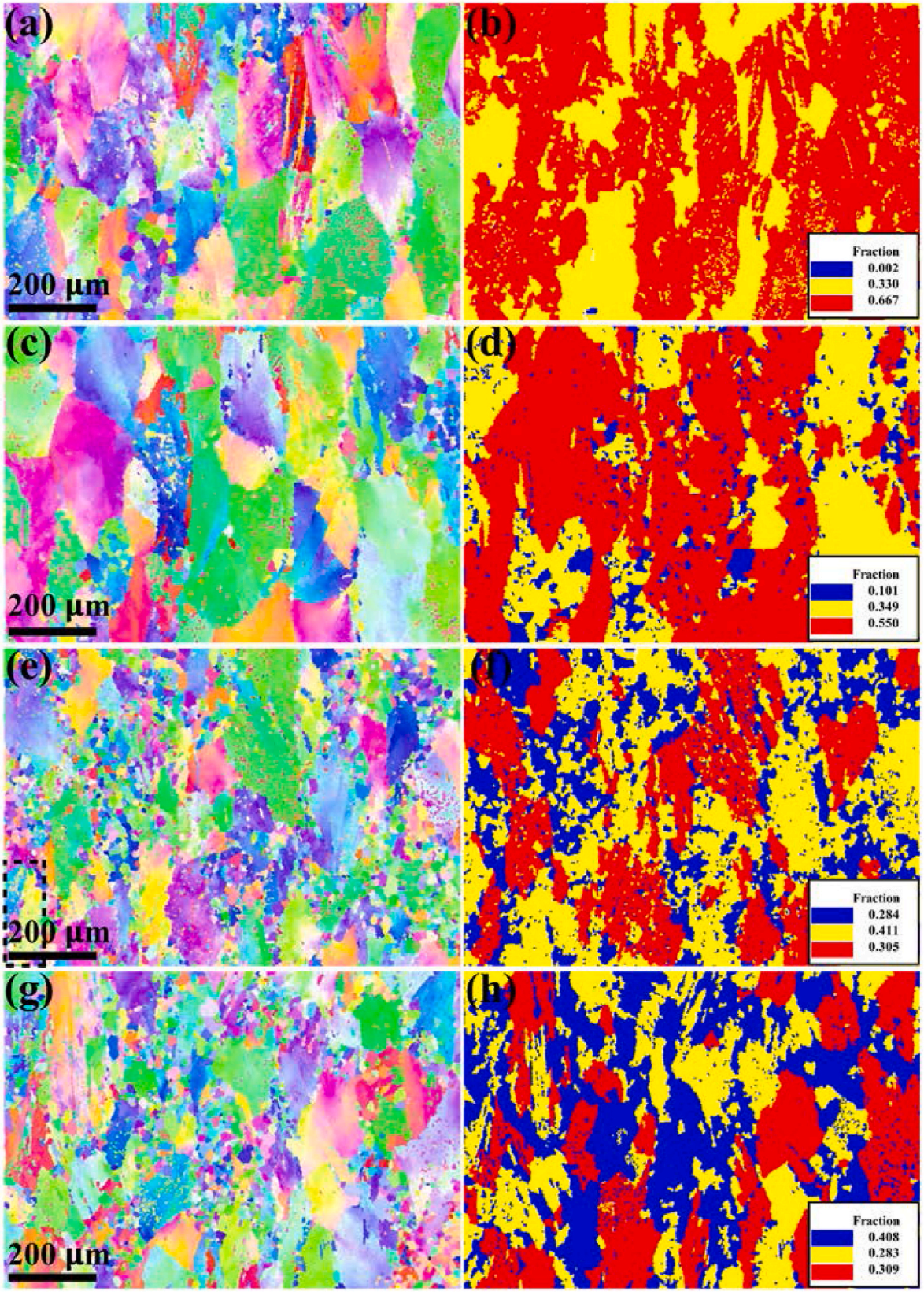

Fig. 5. The IPF and GOS images of cold-rolled sample after annealing at 400 °C for (a,b) 1 min, (c,d) 3 min, (e,f) 4 min, (g,h) 5 min.

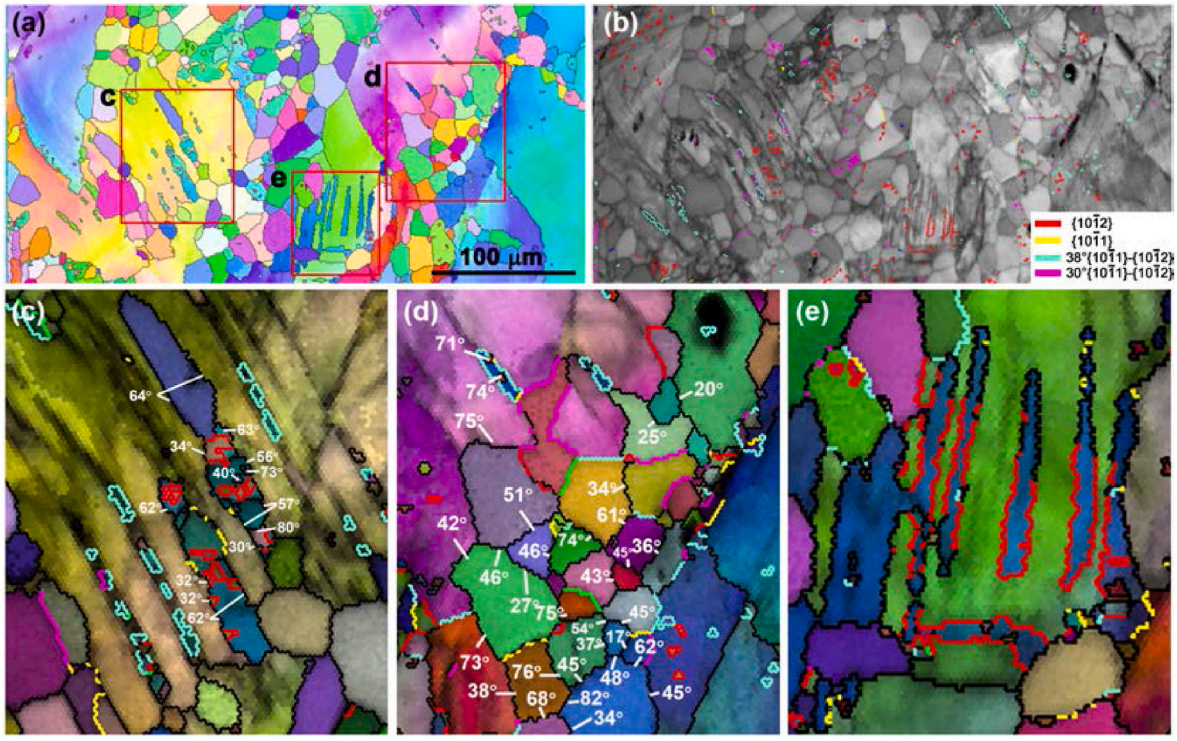

Fig. 6. EBSD results of the sample annealed for 5 min. (a) IPF map, (b) IQ map superimposed with the twin boundary map, (c–e) magnified IPF + IQ maps of areas c, d and e, respectively.

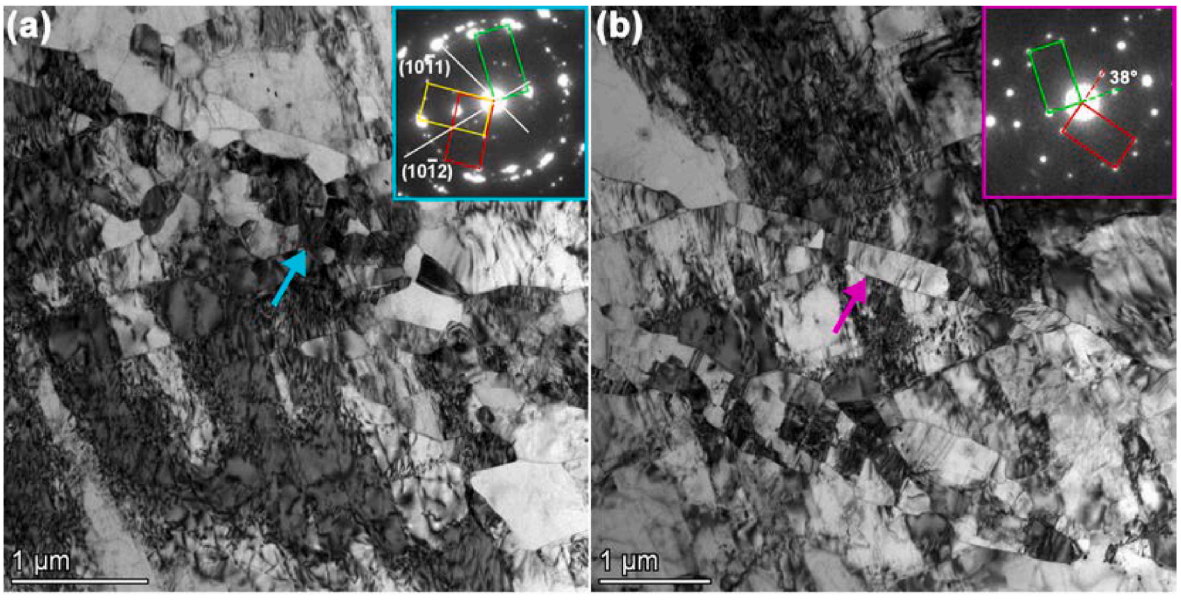

Fig. 7. The bright-field TEM images of local areas containing many recrystallized grains in the annealed specimen. Diffraction patterns of the pointed areas were inserted at the right up corners.

and grain A possess a 38° (with a 2° tolerance) {10$\bar{1}$1}-{10$\bar{1}$2} double twin relation. And the diffraction spots of (0002) plane in grain A is extended, which indicates the formation of small angle grain boundaries due to the cumulative effect of dislocations during deformation and annealing treatment. Fig. 8d–g shows that both the grain A and grain C have a 38° (with a 1.8° tolerance) {10$\bar{1}$1}-{10$\bar{1}$2} double twin relation with the matrix grain. But the grain B between grain A and grain C has a distinct orientation with the matrix, indicating that grain B is a recrystallized grain, nucleating at the boundary of {10$\bar{1}$1}-{10$\bar{1}$2} double twin. Fig. 8f shows that grain D has a {10$\bar{1}$1}-{10$\bar{1}$2} double twin relation with the matrix grain, grain D has a {10$\bar{1}$2} twin relation with the grain F, grain F has a {10$\bar{1}$1} twin relation with the matrix grain M, and grain D has a small angle orientation difference (about 8°) with grain E. The results indicate that the interface between grain D and grain E is a sub-grain boundary, formed due to the large number of dislocations accumulated in the twins during cold rolling and rearranged during annealing process. Fig. 8g shows that grain G has a 38° (with a 2° tolerance) {10$\bar{1}$1}-{10$\bar{1}$2} double twin relation with the matrix grain M,

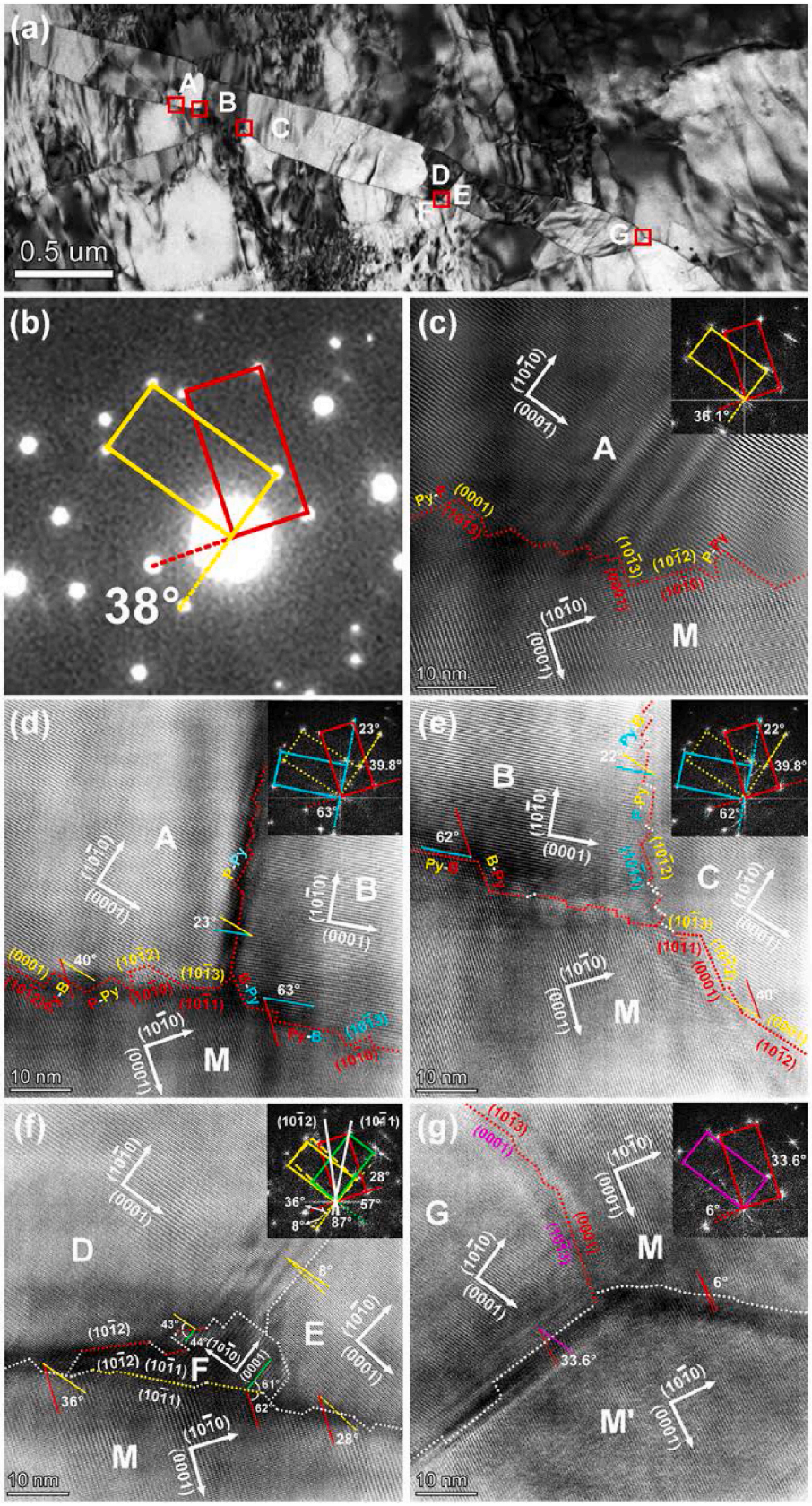

Fig. 8. (a) A bright-field TEM image showing twinning recrystallization. Grains A-G were labeled in a. (b) An SAED pattern showing the $\{10\bar{1}1\}$-$\{10\bar{1}2\}$ double twin relation. (c–g) HRTEM images containing interfaces of these grains as marked by squares and their corresponding FFT patterns.

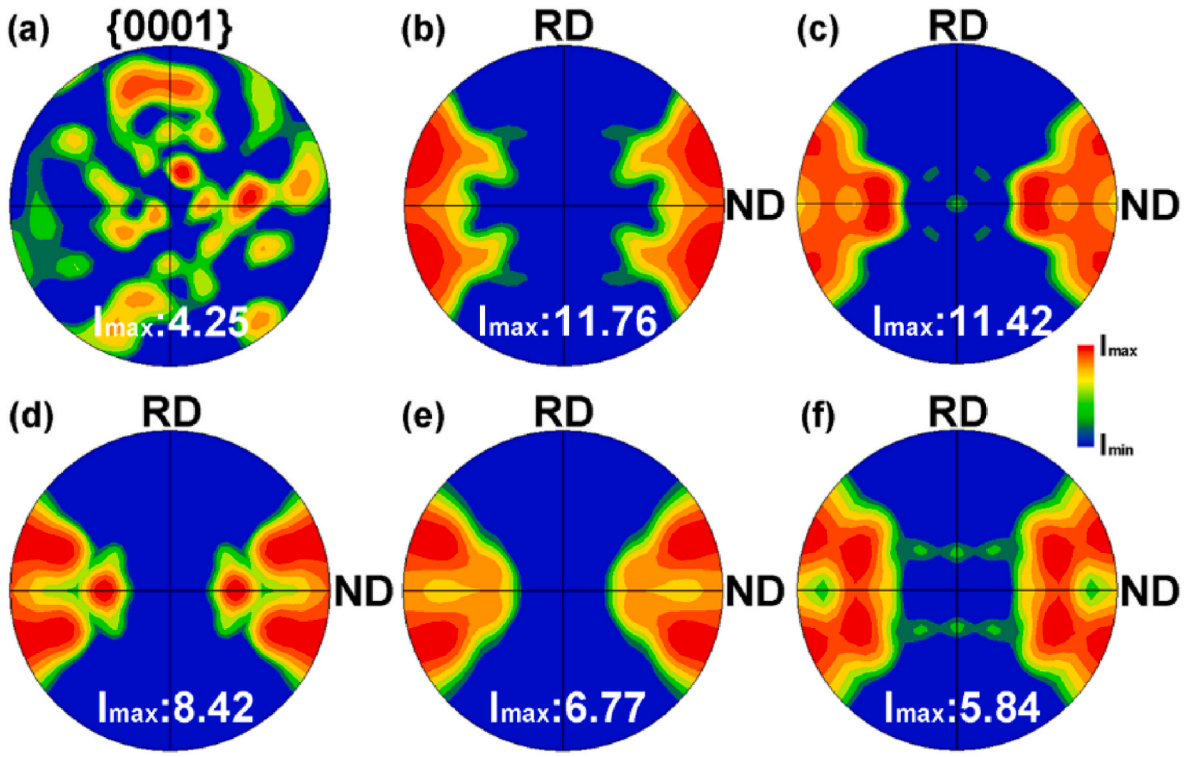

Fig. 9. The {0001} pole figure maps of the homogenized sample (a), cold rolled sample (b), and annealed samples at 400 °C for (c) 1min, (d) 3 min, (e) 4 min and (f) 5 min.

and matrix grain M has a small angle orientation difference (about 6°) with matrix grain M', indicating that dislocation rearrangement also occurred in the matrix forming a low angle grain boundary at the interface of double twin boundary and matrix grain boundary. The results indicate that recrystallization occurs at the double twin boundary and the interface between the double twin boundary and the matrix boundary due to the dislocation movement during annealing.

3.3. Texture evolution during cold rolling and annealing

Fig. 9 shows the {0001} pole figure maps of the homogenized sample (a), cold rolled sample (b), and annealed samples. The homogenized sample has a random grain orientation with multiple peaks in the {0001} pole figure map, as shown in Fig. 9a. Among these peaks, the maximum intensity is about 4.25 mrd. After cold rolling, the {0001} texture of the sample has two concentrated peaks, indicating that the (0001) crystal plane is perpendicular to the normal direction and parallel to the rolling surface. The peak density of the sample after cold rolling is ~11.76 mrd, which indicates a strong basal texture. With the increase of annealing time, the maximum intensity gradually decreases from ~11.76 mrd for the cold rolled sample to ~5.84 mrd for the sample annealed for 5 min.

Fig. 10 shows the evolution of texture of the recrystallized grains for samples annealed for 3 min (a, b), 4 min (c, d) and 5 min (e, f). Obviously, the maximum intensity of the textures is quite different from the whole samples as shown in Fig. 9. It can be seen that the maximum intensity is ~3.12 mrd of the recrystallized grains in the 3 min annealed sample, which also belongs to the basal texture but has much lower intensity than that for the whole grains. The intensity difference indicates that the recrystallized grains weaken the texture of the deformed grains. After annealing for 4 min, the peak intensity of recrystallized texture decreases slightly to ~2.99, indicating that the orientation of recrystallized grains is further dispersed. However, the texture intensity of the recrystallized grains increased slightly in the 5 min annealed sample. The texture evolution will be further analyzed in section 4.2.

3.4. Hardness evolution during annealing treatment

Fig. 11 presents the evolution of hardness of the cold-rolled sample after annealing at 400 °C for different time. Three stages (I, II and III) were defined according to the hardness variation trend with the annealing time. The hardness of the cold rolled sample is ~90 HV. In stage I (1–3 min), the hardness decreased slightly, indicating recovery and a small amount of recrystallization nucleation occurred. In stage II (3–20 min), the hardness decreased significantly, indicating the amount of recrystallized grains increased greatly. In stage III (20–30 min), the hardness decreased slightly. Fully recrystallization was achieved after 20 min annealing, and grain growth occurred with further increase of the annealing time, resulting in the decrease of hardness.

4. Discussion

4.1. Recovery and recrystallization behavior during annealing

The deformed microstructures as shown in Figs. 1–3 indicate that 38° $\{10\bar{1}1\}$-$\{10\bar{1}2\}$ double twins, 56° $\{10\bar{1}1\}$ twins and 86° $\{10\bar{1}2\}$ twins were activated during cold rolling deformation. Generally, $\{10\bar{1}2\}$ twins are produced easily due to a relatively lower critical resolved shear stress of ~ 2–3 MPa [35], compared with a value of 114 MPa for $\{10\bar{1}1\}$ twins [36]. Therefore, $\{10\bar{1}2\}$ twins are the main deformation twins. The driving force of recrystallization is related to the deformation energy. Although $\{10\bar{1}2\}$ twins are the most common twins in Mg alloys, the interface of this type of twin has strong mobility and is easy to expand, making it hard to store high deformation energy within the twins. Therefore, it is generally difficult for a single $\{10\bar{1}2\}$ twin to recrystallize [30]. However, compression twins and double twins are generally difficult to expand and can store high deformation energy, so they are conducive to becoming nucleation sites for recrystallization. Basu et al. [37] found that the intersection of double twins is the most common location where new recrystallized grains usually first nucleate

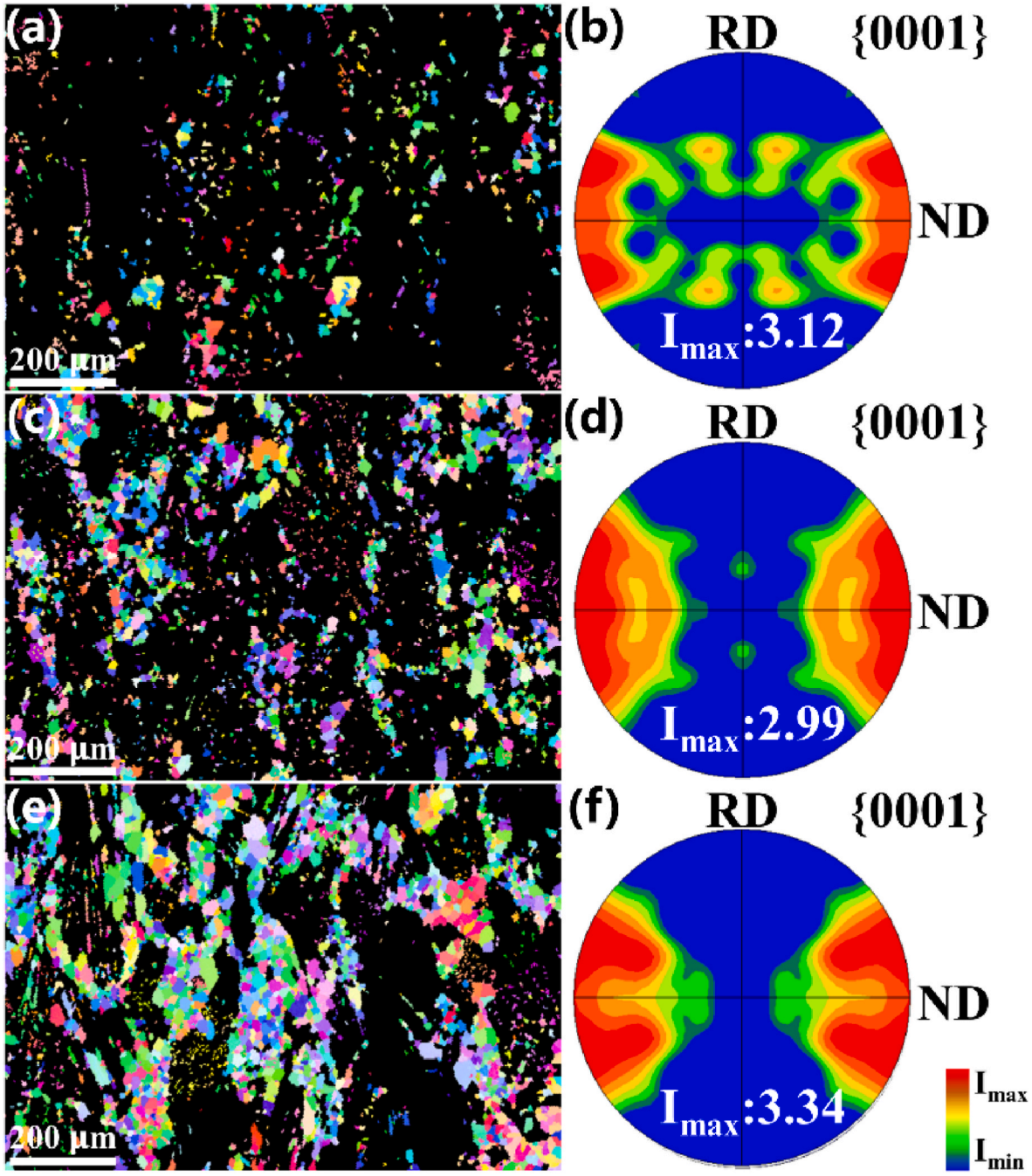

Fig. 10. The evolution of texture of the recrystallized grains for samples annealed for 3 min (a, b), 4 min (c, d) and 5 min (e, f).

due to the inhomogeneous distribution of stress with a relatively high deformation stored energy in localized areas. Therefore, the 38° $\{10\bar{1}1\}$-$\{10\bar{1}2\}$ double twin boundaries are conducive to becoming nucleation sites of recrystallization.

The detailed HRTEM analysis further indicates that recrystallized grains nucleate and grow at the $\{10\bar{1}1\}$-$\{10\bar{1}2\}$ double twin boundaries and the interface of double twin and the matrix by the dislocation rearrangement during annealing treatment, as shown in Fig. 8. The high residual stress introduced in the grains at the initial deformation stage would be the major driving force for the nucleation and growth of recrystallized grains. Nucleation of recrystallization occurs preferentially inside double twins. The nucleation and growth of recrystallized grains is proposed to take place with the help of dislocation slip, whereby the high density of dislocations in double twins and the interface of the double twin and matrix are rearranged into low angle grain boundaries and eventually evolve to high angle boundaries. Moreover, in Mg-RE alloys, the rare earth elements can pin the grain boundaries and twin boundaries, inhibiting the movement of the boundaries, which is conducive to the accumulation of dislocations and stress, and finally contribute to the occurrence of static recrystallization. In addition, Lu et al. [9] found that the interaction of neighboring dislocations in twins and the matrix can pin the twin boundary, reducing the mobility of $\{10\bar{1}2\}$ twin boundaries. As a result, those pinned twin boundaries can also effectively accumulate dislocations and may promote the nucleation of recrystallized grains at the $\{10\bar{1}2\}$ twin boundaries during annealing treatment.

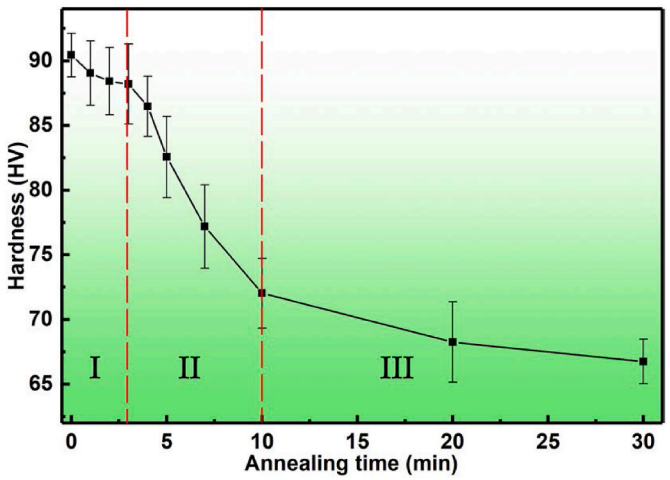

Fig. 11. The hardness evolution of the cold-rolled samples during annealing process.

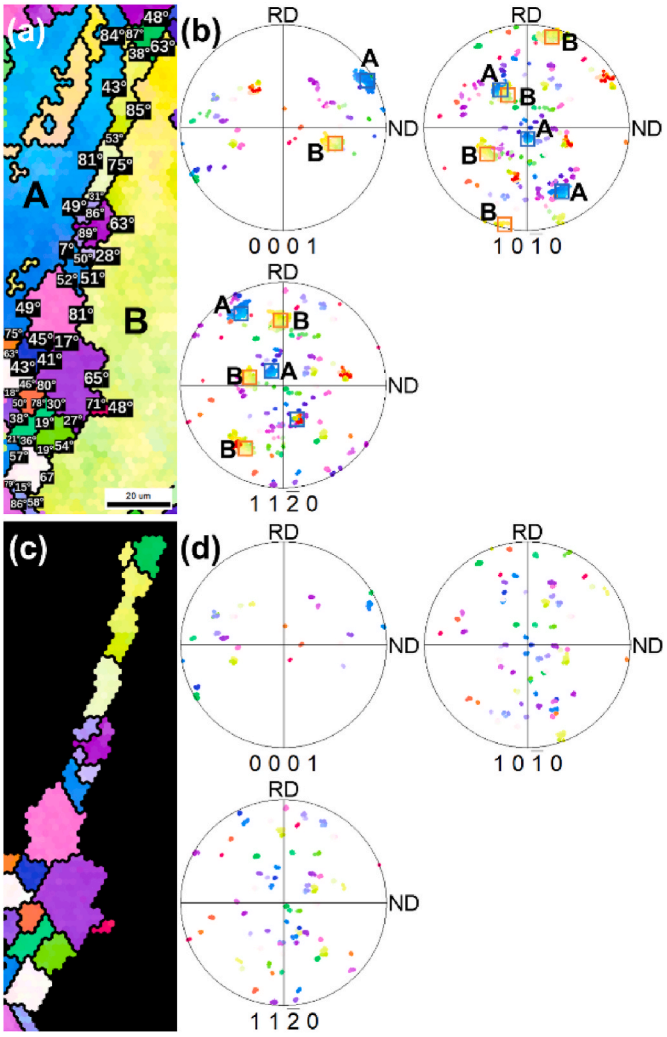

Fig. 12. (a) IPF map with the grain boundary misorientations marked for the un-recrystallized grains A and B, and recrystallized grains between grain A and grain B, (b) orientation distributions in pole figures, (c) IPF map of recrystallized grains, (d) orientation distributions in pole figures of recrystallized grains.

4.2. Texture evolution

It is necessary to study the texture evolution during the deformation and annealing treatments, considering that Mg alloys have limited slip systems, and the texture greatly influences the mechanical properties. As can be seen from Fig. 9, a strong basal texture existed in the cold rolled alloy. Annealing treatment weakened the texture of the cold rolled sample. The maximum texture intensity decreased with the increment of annealing time, for the reason that the fine recrystallized grains produced during static recrystallization weakened the texture of the whole grains, as can be seen from Fig. 10. The recrystallized grains exhibited a much lower texture intensity than the deformed grains (un-recrystallized grains). Yang et al. [38] studied the static recrystallization of Mg-Gd-Y-Zr alloys and found that new fine grains weakened the texture significantly.

To further analyze the texture evolution, the region marked by a black dashed rectangle at the left bottom of Fig. 5e was further enlarged and analyzed in Fig. 12. Fig. 12a shows the IPF map with the grain boundary misorientations marked for the un-recrystallized grains A and B and recrystallized grains between grain A and grain B. Fig. 12b shows the pole figures. Fig. 12c and d are the IPF image and pole figures of the recrystallized grains. Note that there exists a certain number of misorientation angles close to 38° $\{10\bar{1}1\}$-$\{10\bar{1}2\}$ and 86° $\{10\bar{1}2\}$ twins, it is therefore speculated that this region is a recrystallization band generated by nucleation of recrystallized grains at a double twin boundary and a 86° $\{10\bar{1}2\}$ twin boundary, and the recrystallized grains have low angle misorientations with the original twin.

During the annealing treatment, the recrystallized grains preferentially nucleate within the double twins and at the interfaces between the double twin and the matrix. With the increment of annealing time, the recrystallized grains may also nucleate and grow at the $\{10\bar{1}2\}$ twin-twin intersections with the help of the pinning effect caused by rare earth elements, and eventually a group of grains with random orientations will be formed. Though some of the recrystallized grains at the deformed twin band will retain close orientations to the original grains, more recrystallized grains will grow along different orientations and weaken the texture of the whole material.

5. Conclusion

In this study, cold rolling and annealing were conducted on a Mg-5.9Gd-3.3Y-0.5Zr alloy to investigate the recrystallization behavior and texture evolution. The deformed microstructures especially the deformation twins and their effects on static recrystallization and texture evolution were analyzed. The main conclusions can be summarized as follows:

(1) A high density of $\{10\bar{1}2\}$, $\{10\bar{1}1\}$ twins and $\{10\bar{1}1\}$-$\{10\bar{1}2\}$ double twins were introduced in the cold rolled alloy. Twinning recrystallization occurred during subsequent annealing treatment. Complete recrystallization and grain refinement were realized after annealing for 20 min. The 38° $\{10\bar{1}1\}$-$\{10\bar{1}2\}$ double twins and the interfaces of double twins and parent grain boundaries acted as the preferential nucleation sites for the recrystallized grains due to the high stored energy.

(2) During the recrystallization process, the basal texture of the cold rolled sample still existed, but the overall texture intensity was significantly reduced due to the dispersion of grain orientation brought by new grains generated by twin recrystallization. The hardness did not change significantly after annealing for 1–3 min because only recovery and partial recrystallization occurred at this stage. After annealing for 3–20 min, obvious recrystallization nucleation and growth occurred, resulting in significant decrease on hardness.

Credit authors statement

Wenting Jiang: Data curation, Formal analysis, Writing - original draft, Review & Editing., **Xinyu Ren**: Data curation, Formal analysis, Writing - Review &Editing., **Lei Yu**: Data curation, Formal analysis, Writing - original draft, Review & Editing., **Jingli Sun**: Formal analysis, Writing - review & editing., **Song Ni**: Conceptualization, Formal analysis, Writing - Review &Editing, Supervision, Project administration, Funding acquisition., **Yi Huang**: Formal analysis, Writing - Review &Editing., **Min Song**: Formal analysis, Writing - review & editing.

Data availability

All data used during the study are available from the corresponding author by request.

Declaration of competing interest

The authors declare that they have no known competing financial interests or personal relationships that could have appeared to influence the work reported in this paper.

Acknowledgments

We would like to thank the financial support from National Natural Science Foundation of China [grant number 52171130 (S.N.)], Huxiang Youth Talents Support Program [grant number 2021RC3002 (S.N.)]. YH is grateful for support from the Royal Society in the UK under Grant No. IEC\R3\193025. The Advanced Research Center of Central South University is sincerely appreciated for TEM support.

References

[1] Zhang H, Li Y, Liu Y, Zhu Q, Qi X, Zhu G, Wang J, Jin P, Zeng X. The effect of basal <a> dislocation on {11-21} twin boundary evolution in a Mg-Gd-Y-Zr alloy. J Mater Sci Technol 2021;81:212–8. https://doi.org/10.1016/j.jmst.2020.11.062.
[2] Agnew SR, Duygulu Ö. Plastic anisotropy and the role of non-basal slip in magnesium alloy AZ31B. Int J Plast 2005;21(6):1161–93. https://doi.org/10.1016/j.scriptamat.2010.06.029.
[3] Shah SSA, Wu D, Chen RS, Song GS. Temperature effects on the microstructures of Mg–Gd–Y alloy processed by multi-direction impact forging. Acta Metall Sin 2019;33(2):243–51. https://doi.org/10.1007/s40195-019-00972-6.
[4] Guo R, Zhao X, Hu BW, Tian XD, Wang Q, Zhang ZM. Hot compression behavior of Mg–Gd–Y–Zn–Zr alloy containing LPSO with different morphologies. Acta Metall Sin 2023;36(10):1680–98. https://doi.org/10.1007/s40195-023-01587-8.
[5] Zheng R, Bhattacharjee T, Shibata A, Sasaki T, Hono K, Joshi M, Tsuji N. Simultaneously enhanced strength and ductility of Mg-Zn-Zr-Ca alloy with fully recrystallized ultrafine grained structures. Scripta Mater 2017;131:1–5. https://doi.org/10.1016/j.scriptamat.2016.12.024.
[6] Lee HH, Yoon JI, Park HK, Kim HS. Unique microstructure and simultaneous enhancements of strength and ductility in gradient-microstructured Cu sheet produced by single-roll angular-rolling. Acta Mater 2019;166:638–49. https://doi.org/10.1016/j.actamat.2019.01.021.
[7] Wang BJ, Xu DK, Wang SD, Sheng LY, Zeng R-C, Han E-h. Influence of solution treatment on the corrosion fatigue behavior of an as-forged Mg-Zn-Y-Zr alloy. Int J Fatig 2019;120:46–55. https://doi.org/10.1016/j.scriptamat.2011.10.046.
[8] Ma QX, Yang HJ, Wang Z, Shi XH, Liaw PK, Qiao JW. High strength and ductility in partially recrystallized Fe40Mn20Cr20Ni20 high-entropy alloys at cryogenic temperature. Microstructures 2022;2(3). https://doi.org/10.20517/microstructures.2022.12.
[9] Lu SH, Wu D, Chen RS, Han E-h. Microstructure and texture optimization by static recrystallization originating from {10-12} extension twins in a Mg-Gd-Y alloy. J Mater Sci Technol 2020;59:44–60. https://doi.org/10.1016/j.jmst.2020.04.040.
[10] Barrett CD, Imandoust A, Oppedal AL, Inal K, Tschopp MA, El Kadiri H. Effect of grain boundaries on texture formation during dynamic recrystallization of magnesium alloys. Acta Mater 2017;128:270–83. https://doi.org/10.1016/j.actamat.2017.01.063.
[11] Jiang MG, Xu C, Nakata T, Yan H, Chen RS, Kamado S. Development of dilute Mg–Zn–Ca–Mn alloy with high performance via extrusion. J Alloys Compd 2016;668:13–21. https://doi.org/10.1016/j.jallcom.2016.01.195.
[12] Agnew SR, Nie JF. Preface to the viewpoint set on: the current state of magnesium alloy science and technology. Scripta Mater 2010;63(7):671–3. https://doi.org/10.1016/j.scriptamat.2010.06.029.
[13] Drouven C, Basu I, Al-Samman T, Korte-Kerzel S. Twinning effects in deformed and annealed magnesium–neodymium alloys. Mater Sci Eng, A 2015;647:91–104. https://doi.org/10.1016/j.msea.2015.08.090.
[14] Basu I, Al-Samman T. Twin recrystallization mechanisms in magnesium-rare earth alloys. Acta Mater 2015;96:111–32. https://doi.org/10.1016/j.actamat.2015.05.044.
[15] Liu F, Xin R, Wang C, Song B, Liu Q. Regulating precipitate orientation in Mg-Al alloys by coupling twinning, aging and detwinning processes. Scripta Mater 2019;158:131–5. https://doi.org/10.1016/j.scriptamat.2018.08.049.
[16] Nie JF, Zhu YM, Liu JZ, Fang XY. Periodic segregation of solute atomsin fully coherent twin boundaries. Science 2013;340(6135):957–60.
[17] Yu H, Xin Y, Cheng Y, Guan B, Yu HH, Xin YC, Cheng Y, Guan MY, Liu Q. The different hardening effects of tension twins on basal slip and prismatic slip in Mg alloys. Mater Sci Eng, A 2017;700:695–700. https://doi.org/10.1016/j.msea.2017.06.034.
[18] Guo F, Luo X, Xin Y, Wu G, Liu Q. Obtaining high strength and high plasticity in a Mg-3Al-1Zn plate using pre-tension and annealing treatments. J Alloys Compd 2017;704:406–12. https://doi.org/10.1016/j.jallcom.2017.02.087.
[19] Yin DD, Boehlert CJ, Long LJ, Huang GH, Zhou H, Zheng J, Wang QD. Tension-compression asymmetry and the underlying slip/twinning activity in extruded Mg–Y sheets. Int J Plast 2021;136:102878. https://doi.org/10.1016/j.ijplas.2020.102878.
[20] Lu WJ, An FC, Liebscher CH. Detwinning/twin growth-induced phase transformation in a metastable compositionally complex alloy. Microstructures 2022;2(4). https://doi.org/10.20517/microstructures.2022.14.
[21] El Kadiri H, Barrett CD, Wang J, Tomé CN. Why are {10-12} twins profuse in magnesium? Acta Mater 2015;85:354–61. https://doi.org/10.1016/j.actamat.2014.11.033.
[22] Wang BS, Xin RL, Huang GJ, Liu Q. Strain rate and texture effects on microstructural characteristics of Mg-3Al-1Zn alloy during compression. Scripta Mater 2012;66(5):239–42. https://doi.org/10.1016/j.scriptamat.2011.10.046.
[23] Xin R, Guo C, Xu Z, Liu G, Huang X, Liu Q. Characteristics of long {10-12} twin bands in sheet rolling of a magnesium alloy. Scripta Mater 2014;74:96–9. https://doi.org/10.1016/j.scriptamat.2013.11.008.
[24] Ando D, Koike J, Sutou Y. Relationship between deformation twinning and surface step formation in AZ31 magnesium alloys. Acta Mater 2010;58(13):4316–24. https://doi.org/10.1016/j.actamat.2010.03.044.
[25] Li X, Yang P, Wang LN, Meng L, Cui F. Orientational analysis of static recrystallization at compression twins in a magnesium alloy AZ31. Mater Sci Eng, A 2009;517(1–2):160–9. https://doi.org/10.1016/j.msea.2009.03.045.
[26] Levinson A, Mishra RK, Doherty RD, Kalidindi SR. Influence of deformation twinning on static annealing of AZ31 Mg alloy. Acta Mater 2013;61(16):5966–78. https://doi.org/10.1016/j.actamat.2013.06.037.
[27] Marti É, Mishra RK, Jonas JJ. Effect of twinning on recrystallisation textures in deformed magnesium alloy AZ31. Phil Mag 2011;91(27):3613–26. https://doi.org/10.1080/14786435.2011.588613.
[28] Al-Samman T, Molodov KD, Molodov DA, Gottstein G, Suwas S. Softening and dynamic recrystallization in magnesium single crystals during c-axis compression. Acta Mater 2012;60(2):537–45. https://doi.org/10.1016/j.actamat.2011.10.013.
[29] Jäger A, Lukáč P, Gärtnerová V, Haloda J, Dopita M. Influence of annealing on the microstructure of commercial Mg alloy AZ31 after mechanical forming. Mater Sci Eng, A 2006;432(1–2):20–5. https://doi.org/10.1016/j.msea.2006.06.070.
[30] Guan D, Rainforth WM, Ma L, Wynne B, Gao J. Twin recrystallization mechanisms and exceptional contribution to texture evolution during annealing in a magnesium alloy. Acta Mater 2017;126:132–44. https://doi.org/10.1016/j.actamat.2016.12.058.
[31] Lu SH, Wu D, Chen RS, Han E-H. Reasonable utilization of {10-12} twin for optimizing microstructure and improving mechanical property in a Mg-Gd-Y alloy. Mater Des 2020;191. https://doi.org/10.1016/j.matdes.2020.108600.
[32] Zeng ZR, Zhu YM, Xu SW, Bian MZ, Davies CHJ, Birbilis N, Nie JF. Texture evolution during static recrystallization of cold-rolled magnesium alloys. Acta Mater 2016;105:479–94. https://doi.org/10.1016/j.actamat.2015.12.045.
[33] Al-Samman T, Gottstein G. Dynamic recrystallization during high temperature deformation of magnesium. Mater Sci Eng, A 2008;490:411–20. https://doi.org/10.1016/j.msea.2008.02.004.
[34] Liu YX, Li YX, Zhang H, Zhu QC, Qi XX, Wang J, Wang JH, Jin PP, Zeng XP. Influence of twinning-induced recrystallization on texture evolution in a high strain rate compressed Mg-Zn alloy. Mater Char 2020;162:110192. https://doi.org/10.1016/j.matchar.2020.110192.
[35] Barnett ZK, Ma X. A semianalytical sachs model for the flow stress of a magnesium alloy. Metall Mater Trans A 2006;37A(2283).
[36] Koike J, Sato Y, Ando D. Origin of the anomalous {10-12} twinning during tensile deformation of Mg alloy sheet. Mater Trans 2008;49(12):2792–800. https://doi.org/10.2320/matertrans.MRA2008283.
[37] Basu I, Al-Samman T. Competitive twinning behavior in magnesium and its impact on recrystallization and texture formation. Mater Sci Eng, A 2017;707:232–44. https://doi.org/10.1016/j.msea.2017.09.053.
[38] Yang Y, Yang X, Xiao Z, Zhang D, Wang J, Sakai T. Annealing behavior of a cast Mg-Gd-Y-Zr alloy with necklace fine grains developed under hot deformation. Mater Sci Eng, A 2017;688:280–8. https://doi.org/10.1016/j.msea.2017.02.008.